Journal of Controlled Release 328 (2020) 640–652

Contents lists available at ScienceDirect

Journal of Controlled Release

journal homepage: www.elsevier.com/locate/jconrel

Fibroblast growth factor 2 conjugated superparamagnetic iron oxide nanoparticles (FGF2-SPIONs) ameliorate hepatic stellate cells activation in vitro and acute liver injury in vivo

Dhadhang Wahyu Kurniawan[a,b], Richell Booijink[a], Lena Pater[a], Irene Wols[a], Aggelos Vrynas[a], Gert Storm[a,c], Jai Prakash[a,1], Ruchi Bansal[a,*,1]

[a] Department of Biomaterials Science and Technology, Technical Medical Centre, Faculty of Science and Technology, University of Twente, Enschede, the Netherlands
[b] Department of Pharmacy, Universitas Jenderal Soedirman, Purwokerto, Indonesia
[c] Department of Pharmaceutics, Utrecht Institute of Pharmaceutical Sciences, Faculty of Science, Utrecht University, Utrecht, the Netherlands

ARTICLE INFO

Keywords:
Fibroblast growth factor 2
Super-paramagnetic iron-oxide nanoparticles
Hepatic stellate cells
Liver fibrogenesis
Transforming growth factor beta

ABSTRACT

Liver diseases are the growing health problem with no clinically approved therapy available. Activated hepatic stellate cells (HSCs) are the key driver cells responsible for extracellular matrix deposition, the hallmark of liver fibrosis. Fibroblast growth factor 2 (FGF2) has shown to possess anti-fibrotic effects in fibrotic diseases including liver fibosis, and promote tissue regeneration. Among the fibroblast growth factor receptors (FGFRs), FGF2 interact primarily with FGFR1, highly overexpressed on activated HSCs, and inhibit HSCs activation. However, FGF2 poses several limitations including poor systemic half-life and stability owing to enzymatic degradation. The aim of this study is to improve the stability and half-life of FGF2 thereby improving the therapuetic efficacy of FGF2 for the treatment of liver fibrosis. We found that FGFR1-3 mRNA levels were overexpressed in cirrhotic human livers, while FGFR1c, 2c, 3c, 4 and FGF2 mRNA levels were overexpressed in TGFβ-activated HSCs (LX2 cells) and FGFR1 protein expression was highly increased in TGFβ-activated HSCs. Treatment with FGF2 inhibited TGFβ-induced HSCs activation, migration and contraction in vitro. FGF2 was conjugated to superparamagnetic iron-oxide nanoparticles (SPIONs) using carbodiimide chemistry, and the resulting FGF2-SPIONs were confirmed by dynamic light scattering (DLS), zeta potential, dot-blot analysis and Prussian Blue iron-staining. In vitro, treatment with FGF2-SPIONs evidenced increased therapeutic effects (attenuated TGFβ-induced HSCs activation, migration and contraction) of FGF2 in TGFβ-activated HSCs and ameliorated early liver fibrogenesis in vivo in acute carbon tetrachloride (CCl_4)-induced liver injury mouse model. In contrast, free FGF2 showed no significant effects in vivo. Altogether, this study presents a promising therapeutic approach using FGF2-SPIONs for the treatment of liver fibrosis.

1. Introduction

Liver diseases caused by viral infections (mainly hepatitis B and C viruses), metabolic disorders, alcohol or drug abuse and autoimmune disorders affecting millions of people, represents a major health problem associated with high morbidity and mortality [1]. Acute liver injury is a transient, often reversible, wound healing response however persistent chronic injury to the liver results in progressive accumulation of extracellular matrix (ECM) components eventually resulting in liver cirrhosis, end-stage liver failure and hepatocellular carcinoma [2,3]. Due to the lack of effective therapy, liver diseases poses a major clinical challenge with an increasing number of patients requiring liver transplantation [1,4,5].

Hepatic stellate cells (HSCs) play a key role in the progression of liver fibrosis, regardless of the underlying cause [3,6,7]. Upon injury, hepatocytes undergo apoptosis or necrosis and release pro-inflammatory and pro-fibrogenic mediators that stimulate recruitment and activation of inflammatory cells in the liver resulting in chronic liver inflammation. The resident and infiltrated immune cells, in turn, secrete pro-inflammatory and pro-fibrogenic factors that activate quiescent HSCs [2,3]. Quiescent HSCs transdifferentiate into myofibroblast-like cells and become highly proliferative, migratory and

* Corresponding author: Translational Liver Research, Department of Medical Cell BioPhysics, Technical Medical Centre, Faculty of Science and Technology, University of Twente, 7500 AE Enschede, the Netherlands.
E-mail address: r.bansal@utwente.nl (R. Bansal).
[1] Equal contribution

https://doi.org/10.1016/j.jconrel.2020.09.041
Received 20 April 2020; Received in revised form 1 September 2020; Accepted 20 September 2020
Available online 24 September 2020

contractile cells producing excessive amounts of ECM components that accumulates in the liver parenchyma, disrupting liver architecture and forming the characteristic scar tissue [3,6,7].

Fibroblasts growth factors (FGFs) have been shown to regulate HSCs differentiation and liver fibrosis. There are seven subfamilies of FGFs: FGF1 subfamily (FGF1, FGF2); FGF4 subfamily (FGF4, FGF5, FGF6); FGF8 subfamily (FGF8, FGF17, FGF18); FGF9 subfamily (FGF9, FGF16, FGF20); FGF10 subfamily (FGF3, FGF7, FGF10, FGF22); FGF11 subfamily (FGF11, FGF12, FGF13, FGF14) and FGF19 subfamily (FGF15, FGF19, FGF21, FGF23) [8,9]. These subfamilies of FGFs are tissue specific and have different binding affinities with FGF receptors (FGFRs). There are four isoforms of FGFRs: FGFR1, FGFR2, FGFR3, and FGFR4 that have different splice variants and display tissue specific expression [8,9]. FGF-FGFR signaling is critical in several developmental processes including cellular proliferation, migration, differentiation, morphogenesis and organogenesis [10]. Furthermore, FGF-FGFR signaling pathways regulate liver homeostasis by regulating metabolism of lipids, cholesterol and bile acids, promoting hepatocyte proliferation and detoxification, and facilitating liver regeneration after partial hepatectomy [11].

Among other FGFs, FGF2 (also known as basic FGF) plays a crucial role in numerous cellular processes including organ development, wound healing and tissue regeneration [12]. FGF2 has been shown to regulate HSCs function and has been investigated in liver fibrosis however showed contradictory results [9,13]. Some studies have indicated the pro-fibrotic effects of FGF2, while numerous studies have demonstrated the anti-fibrotic effects of FGF2 in vitro and in vivo in preclinical animal models [13]. Using $FGF1^{-/-}FGF2^{-/-}$ mouse models, Yu et al., demonstrated that acute carbon-tetrachloride (CCl_4) administration in $FGF1^{-/-}FGF2^{-/-}$ mice resulted in elevated serum alanine aminotransferases (ALT) levels, HSCs activation marked by increased intra-hepatic expression of alpha smooth muscle actin (α-SMA) and desmin, accompanied with activation and migration of HSCs to the site-of-injury, while chronic CCl_4 administration led to decreased collagen expression and fibrosis [14]. Pan et al., has demonstrated that 18 KDa low- ($FGF2^{lmw}$) and 21 or 22 KDa high-molecular weight ($FGF2^{hmw}$) forms have distinct role in liver fibrogenesis, and that the exogenous $FGF2^{lmw}$ treatment attenuated HSCs activation and fibrosis [15]. The presence of different FGF2 isoforms with distinct roles might explain the conflicting results reported on the effects of FGF2. Besides hepatic fibrosis, FGF2 treatment has also shown to attenuate bleomycin-induced pulmonary fibrosis [16] and ischemia reperfusion induced renal injury [17].

With respect to myofibroblast (activated HSCs in liver) activation and differentiation, evidences have revealed that FGF2 promotes myofibroblast apoptosis in vivo, antagonizes activation and transforming growth factor beta (TGFβ) signaling, antagonizes contractile phenotypes and myofibroblast differentiation of non-fibroblasts progenitors, suppresses pro-fibrogenic gene expression, and promotes regenerative healing [13]. Mapping studies and crystal structures of FGF-FGFR complexes have revealed that FGF2 binds to different FGFR splice variants with varying affinity [18–20]. In human liver myofibroblasts, FGF2 has been shown to interact with FGFR1 which is highly over-expressed on myofibroblasts [21]. Although the underlying mechanism through which FGF2 affects liver fibrosis is not entirely understood, different FGF2-regulated signaling pathways have been proposed in several diseases and cell types including Janus kinase (JAK), signal transducer and activator of transcription (STAT), extracellular signal regulated kinase (ERK), mitogen-activated protein kinase (MAPK), c-jun N-terminal kinase (JNK) and serine/threonine kinase AKT (also known as protein kinase B, PKB) pathways [13]. Particularly, it has been demonstrated that selective inhibitor of phosphatidylinositol 3-kinase (PI3K) and mitogen-activated protein kinase kinase (MAPKK or MEK) abolished the protective effects of FGF2 suggesting involvement of PI3K/AKT and MEK/ERK signaling pathways in FGF2-mediated effects [17].

While the attractiveness of using FGF2 as therapeutic is evident, there are several limitations including a short systemic half-life after intravenous administration (due to small size) and poor stability (owing to susceptibility to degradation by proteases) [22]. Conjugation of FGF2 to superparamagnetic iron-oxide nanoparticles (SPIONs) could be a promising alternative for eliminating the drawbacks hampering future clinical application. SPIONs possess tailored surface chemistry, low cytotoxicity and unique magnetic properties [23,24]. Recent developments of polymer (dextran/PEG)-coated SPIONs have shown tremendous improvements in biocompatibility and blood circulation. We have previously demonstrated an increased magnetic resonance imaging (MRI) contrast and therapeutic efficacy using Relaxin-SPIONs in liver fibrosis [25].

In this study, we have first analysed the expression of FGFR in human liver cirrhosis and TGFβ-activated human HSCs (LX cells) in vitro. We then investigated the effects of human recombinant FGF2 (low-molecular weight) on TGFβ-activated human HSCs (LX2 cells) in vitro. In order to improve the stability and systemic half-life of FGF2 thereby therapeutic efficacy, we conjugated FGF2 to dextran- and PEG-coated SPIONs. Subsequently, we examined the therapeutic effects of FGF2-SPIONs versus free FGF2 on TGFβ-activated human HSCs in vitro and in an acute CCl_4 induced mouse model in vivo.

2. Materials and methods

2.1. FGFR gene expression analysis in the liver tissues from healthy and cirrhosis patients

Publicly available transcriptome datasets of liver tissues (GSE6764) from normal healthy individuals (n = 10) and cirrhotic patients (n = 12) [26] were analysed using the Gene Expression Omnibus (GEO) database of the National Centre for Biotechnology Information (NCBI) to assess FGF receptor (FGFR) gene expression i.e. FGFR1, FGFR2, FGFR3, FGFR4 and FGF2 in normal and cirrhotic human livers.

2.2. Cell lines

Human hepatic stellate cells (LX2 cells), an immortalized human derived cell line, was provided by Prof. Scott Friedman (Mount Sinai Hospital, New York, NY, USA). LX2 cells were cultured in Dulbecco's Modified Eagle's Medium (DMEM)-Glutamax (Invitrogen, Carlsbad, CA, USA) supplemented with 10% fetal bovine serum (FBS, Lonza, Verviers, Belgium), 50 U/mL penicillin (Sigma, St. Louis, MO, USA) and 50 μg/mL streptomycin (Sigma).

2.3. Conjugation of FGF2 to SPIONs

Human FGF2 (Peprotech, Rocky Hill, NJ, USA) was conjugated to dextran-coated PEG-COOH functionalized super-paramagnetic iron-oxide nanoparticles, SPIONs (micromod Partikeltechnologie, GmbH, Rostock, Germany) using carbodiimide chemistry as described previously [25,27] and depicted in Fig. 5A. Briefly, 100 μL of SPIONs (5 mg/mL) were activated with 35 μmol NHS (N-hydroxysuccinimide, Sigma) and 10 μmol EDC (1-ethyl-3-(3-dimethylaminopropyl)-carbodiimide HCl, Sigma) prepared in 125 μL of MES ([2(-N-morpholino) ethanesulfonic acid, Sigma) buffer (pH 6.3). After 45 min of reaction at RT with gentle shaking, SPIONs were washed thrice with PBS and purified using 30 kDa Amicon™ Ultra Centrifugal Filters (Merck Millipore, Darmstadt, Germany) by centrifugation at 5000 rpm. Afterwards, 15 μg of FGF2 (0.06 nmol in 15 μL) was added to the activated SPIONs and left to react for overnight at 4 °C with gentle shaking. Samples were then purified and unconjugated COOH groups (on SPIONs) were reacted with 10 μg of glycine (Sigma) for 30 min at RT. Eventually, FGF2-coated SPIONs (FGF2-SPIONs) were purified, resuspended in 100 μL PBS and stored at 4 °C.

2.4. Characterization of FGF2-SPIONs

2.4.1. Size and zeta potential measurements

The size of SPIONs and FGF2-SPIONs was measured using dynamic light scattering (DLS) with Zetasizer Nano (Malvern Instruments, UK). Briefly, 5 μL of SPIONs or FGF2-SPIONs were diluted in 1 mL PBS and measured in 1 mL disposable polystyrene cuvettes. For zeta potential measurements, 5 μL of SPIONs or FGF2-SPIONs were diluted in 1 mL KCl (10 mM) and measured in folded capillary cells DTS1060 (Malvern Instruments).

2.4.2. Dot blot analysis

Conjugation efficiency of FGF2 on SPIONs was determined by Dot blot analysis as reported previously [25, 27]. Briefly, FGF2, SPIONs and FGF2-SPIONs were serially diluted in TBS buffer (Thermo Scientific, Rockford, IL, USA). 2 μL of the samples were spotted on the nitrocellulose membrane and allowed to dry for 10 min. The membrane was blocked for 1 h with 5% blotting-grade blocker (BioRad, Hercules, CA, USA) prepared in TBS buffer Tween®-20 (TBST) (Thermo Scientific). Afterwards, the membrane was incubated with rabbit anti-FGF2 monoclonal antibody (1:1000; Cell Signaling Technology, Massachusetts, MA, USA) for 1 h. The membrane was washed three times in TBST and incubated for 1 h with secondary rabbit anti-rat HRP-conjugated polyclonal antibody (1:1000, Dako, Glostrup, Denmark) followed by tertiary goat-anti rabbit anti-rat HRP-conjugated polyclonal antibody (1:1000, Dako). Afterwards, the blot was developed using Pierce™ ECL Plus Western Blotting substrate (Thermo Scientific) and was imaged using FluorChem Imaging System (ProteinSimple, Alpha Innotech, San Leandro, CA, USA). The intensity of the dots was quantified using NIH ImageJ software (NIH, Bethesda, MD) and the conjugation efficiency was calculated using the standard curves prepared from known concentrations of FGF2 dots.

2.4.3. Prussian blue iron staining

To estimate the recovery of SPIONs during the conjugation process, Prussian Blue staining kit (Sigma) was performed on the dot blots as per the manufacturer's instructions and described previously [25,27]. Briefly, FGF2, SPIONs and FGF2-SPIONs were serially diluted in TBS buffer (Thermo Scientific). 2 μL of the samples were spotted on the nitrocellulose membrane and allowed to dry for 10 min. Iron was detected using Prussian Blue staining kit (Sigma) containing potassium ferrocyanide and hydrochloric acid in 1:1 ratio. Images were captured using a normal digital camera. The intensity of the dots were quantified using NIH ImageJ software (NIH, Bethesda, MD) and the amount of iron staining (representative of SPIONs) was calculated using the standard curves prepared from known amounts of SPIONs dots.

2.5. Cell binding and uptake experiments

Cell binding and uptake studies were performed as per the standardized protocols reported previously [25]. Briefly, LX2 cells were seeded at 1×10^4 cells/well and cultured overnight. Cells were then serum-starved for overnight and then incubated with 5 ng/mL TGFβ1 (Roche, Mannheim, Germany) for 24 h. TGFβ-activated LX2 cells were then incubated with SPIONs or FGF2-SPIONs at RT for 2 h (binding study) or at 37 °C for 4 h (uptake study) in serum-free medium supplemented with 0.5% BSA (bovine serum albumin). After incubation, cells were washed thrice with Dulbecco's phosphate buffer saline (DPBS, Lonza) and were fixed with 4% formalin and stained using Prussian Blue iron staining as per manufacturer's instructions. Images were captured using Nikon E400 microscope (Nikon, Tokyo, Japan), cellular uptake was assessed by counting iron-positive cells/per field and has been depicted as % uptake.

2.6. Immunofluorescent staining

Cells were seeded in 24-well plates (3×10^4 cells/well) and cultured overnight. Cells were then serum-starved for overnight and incubated with either starvation medium alone, different concentrations of FGF2 (50 ng/mL, 100 ng/mL or 250 ng/mL) or 250 ng/mL FGF2, SPIONs, or FGF2-SPIONs, and 5 ng/mL TGFβ1 for 24 h. Afterwards the cells were washed with 1 x PBS, fixed with ice-cold acetone and methanol (1: 1 ratio) for 30 min at −20 °C followed by drying for 30 min at RT and rehydration with 1× PBS. The staining was performed using rabbit anti-FGFR1 (1:100) or goat anti-collagen I (1:100). Briefly, cells were incubated with the respective primary antibodies (refer to Table S1) followed by incubation with Alexa 488-conjugated secondary antibodies (Life Technologies, Gaithersburg, MD, USA). Cells were then mounted with DAPI-containing mounting medium (Sigma). The staining was visualized, the images were captured using fluorescent microscopy (Evos microscope, Tokyo, Japan), analysed using NIH ImageJ software and presented as relative expression versus TGFβ-treated LX2 cells.

2.7. Cell viability studies

Cells were seeded in 96-well plates (5000 cells/well) and cultured overnight. Cells were serum-starved for overnight and incubated with starvation medium alone, different concentrations of FGF2 (50 ng/mL, 100 ng/mL or 250 ng/mL) or 250 ng/mL FGF2, SPIONs, or FGF2-SPIONs, and 5 ng/mL TGFβ1 for 24 h. Cells were then incubated with Alamar blue reagent (Invitrogen), incubated for 4 h and fluorescent signal was measured using a VIKTOR™ plate reader (Perkin Elmer, Waltham, MA).

2.8. Western blot analysis

Cells were seeded in 12-well plates (8×10^4 cells/well) and cultured overnight. Cells were serum-starved for overnight and incubated with starvation medium alone, different concentrations of FGF2 (50 ng/mL, 100 ng/mL or 250 ng/mL) or 250 ng/mL FGF2, SPIONs, or FGF2-SPIONs, and 5 ng/mL TGFβ1 for 24 h. Cells were lysed using 1× lysis buffer prepared from 3× blue loading buffer and 30× reducing agent (1.25 M dithiothreitol, DTT) (Cell Signaling Technology, Massachusetts, MA, USA) as per manufacturer's instructions. The prepared samples were loaded on 10% Tris-glycine gels (Life Technologies) followed by transfer to the PVDF membrane (Roche). The membranes were developed according to the standard protocols using primary and secondary antibodies (refer to Table S1). The bands were visualized using Pierce™ ECL Plus Western Blotting substrate (Thermo Scientific) and photographed using FluorChem Imaging System. Intensity of individual bands was quantified using NIH ImageJ software, normalized with respective β-actin bands and presented as relative expression versus TGFβ-treated LX2 cells.

2.9. Quantitative real time PCR

Cells were seeded in 12-well plates (8×10^4 cells/well) and cultured overnight. Cells were then serum-starved for overnight and incubated with starvation medium alone, different concentrations of FGF2 (50 ng/mL, 100 ng/mL or 250 ng/mL) or 250 ng/mL FGF2, SPIONs, or FGF2-SPIONs, and 5 ng/mL TGFβ1 for 24 h. Cells were then lysed using RNA lysis buffer. Total RNA from cells was isolated using the GenElute Total RNA Miniprep Kit (Sigma) according to the manufacturer's instructions. The RNA concentration was quantified using NanoDrop® ND-1000 Spectrophotometer (Thermo Scientific, Waltham, USA). Total RNA (1 μg) was reverse transcribed using the iScript cDNA Synthesis Kit (Bio-Rad, Hercules, CA, USA). Real-time PCR was performed using 20 ng of cDNA, pre-tested gene-specific primer sets (listed in Tables S2) and the 2× SensiMix SYBR and Fluorescein Kit (Bioline

GmbH, QT615-05, Luckenwalde, Germany) according to the manufacturer's instructions. Finally, cycle threshold (Ct) values were normalized to the reference gene 18 s rRNA, and relative expression were calculated using the $2^{-\Delta\Delta Ct}$ method versus TGFβ-treated LX2 cells.

2.10. 3D collagen gel cell contraction assay

A collagen suspension (5 mL) containing 3 mL of collagen G1 (5 mg/mL, Matrix biosciences, Morlenbach, Germany), 0.5 mL of 10× M199 medium (Sigma), 85 μL of 1 N NaOH (Sigma) and sterile water was mixed with 1 mL (2×10^6) of LX2 cells. The gel and cell suspension (0.6 mL/well) were plated in a 24-well culture plate and was allowed to polymerize. Polymerized gels were incubated with 1 mL of serum-starved medium with or without human recombinant TGFβ1 (5 ng/mL) together with different concentrations of FGF2 (50 ng/mL, 100 ng/mL or 250 ng/mL), or 250 ng/mL of FGF2, FGF2-SPIONs, and SPIONs (equimolar concentration), followed by detachment of the gels. Digital images were made after 72 h of treatment using a normal digital camera. The size of the gels was digitally measured using NIH ImageJ software, and were normalized with their respective well size (measured using NIH ImageJ software) in each image and presented as relative gel contraction versus TGFβ-treated LX2 cells.

2.11. Cell migration assay

Cells were plated in 12-well culture plates (1×10^5 cells/well), cultured overnight and serum-starved for 24 h. A standardized scratch was made using a 200 μL pipette tip fixed in a custom-designed holder. Afterwards, cells were washed twice and incubated with starvation medium (control), or with 5 ng/mL TGFβ1 prepared with or without different concentrations of FGF2 (50 ng/mL, 100 ng/mL or 250 ng/mL), or 250 ng/mL FGF2, SPIONs, or FGF2-SPIONs. Microscopic images were taken at 0 and 24 h to measure the size of the scratch. The images acquired for each sample were analysed quantitatively using NIH ImageJ software. For each image, an area between one side of scratch and the other was measured at time 0 and 24 h to obtain the scratch closure on the basis of the areas that were measured using ImageJ software. Graph represents relative wound healing versus TGFβ-treated LX2 cells.

2.12. CCl_4-induced acute liver injury mouse model

All the animal experiments were carried out strictly according to the ethical guidelines for the Care and Use of Laboratory Animals (Utrecht University, The Netherlands). Male Balb/c mice (8–10 weeks old) received single intraperitoneal injection of 1.0 mL/kg carbon tetrachloride (CCl_4, Sigma) at day 1. CCl_4-treated mice were treated with two intravenous administrations of PBS ($n = 5$), FGF2 (250 ng/dose, $n = 5$) or FGF2-SPIONs (250 ng/dose, $n = 6$) at day 3 and day 5. Healthy controls ($n = 6$) received olive oil alone. All the animals were euthanized at day 6. Liver tissues and blood samples were retrieved for further analyses. All the animals were weighed before sacrificing, and the respective organs were weighed directly after sacrificing. Alanine aminotransferase (ALT) activity was determined in the plasma samples using a colorimetric ALT activity assay kit (Sigma MAK052) according to the manufacturer's instructions.

2.13. Histological immunostainings

Collected liver tissues were transferred to Tissue-Tek OCT embedding medium (Sakura Finetek, Torrance, CA, USA) and snap-frozen in 2-methyl butane in a dry ice. Cryosections (5 μm) were cut using a Leica CM 3050 cryostat (Leica Microsystems, Nussloch, Germany). The cryosections were air-dried and fixed with acetone for 20 min. Tissue sections were rehydrated with PBS and incubated with the primary antibody (Collagen I or F4/80) overnight at 4 °C (refer to Table S1). This was followed by incubation with horseradish peroxidase (HRP)-conjugated secondary antibody for 1 h at RT. Next, the samples were incubated with HRP-conjugated tertiary antibody for 1 h at RT. Thereafter, peroxidase activity was developed using the AEC (3-amino-9-ethyl carbazole) substrate kit (Life Technologies) for 20 min and nuclei were counterstained with hematoxylin (Fluka Chemie, Buchs, Switzerland). Endogenous peroxidase activity was blocked by 3% H_2O_2 prepared in methanol. The sections were mounted with Aquatex mounting medium (Merck) and were scanned using Hamamatsu NanoZoomer Digital slide scanner 2.0 HT (Hamamatsu Photonics). For quantitation, the high resolution scans were viewed using NanoZoomer Digital Pathology (NDP2.0) viewer software (Hamamatsu Photonics). About 20 images (100×) of each stained liver tissue section (from NDP) were imported into ImageJ software and were analysed quantitatively at a fixed threshold.

2.13.1. Prussian blue staining combined with collagen I immunostaining

Cryosections were dried and fixed with 4% formaldehyde (Sigma) for 30 min. The sections were washed thrice with 1× PBS and incubated with primary collagen I antibody for 1 h at RT, followed by incubation with 0.3% hydrogen peroxide for 30 min. Next, the sections were incubated with horseradish peroxidase (HRP)-conjugated secondary antibody for 1 h and HRP-conjugated tertiary antibody for 1 h. Sections were then stained with AEC for 20 min as per manufacturer's instructions. Thereafter, the sections were washed with Milli Q water and incubated with freshly prepared Prussian blue solution (Sigma). The sections were incubated with Prussian blue mix solution for 30 min, washed in deionized water followed by mounting with aquatex mounting medium, and imaged using NanoZoomer.

2.14. Graphs and statistical analyses

All graphs were made using GraphPad Prism version 8.4.1 (GraphPad Prism, La Jolla, CA, USA). The results are expressed as the mean + standard error of the mean (SEM). Statistical analyses were performed using GraphPad Prism version 8.4.1 (GraphPad Prism, La Jolla, CA, USA). Multiple comparisons between different groups were calculated using the one-way analysis of variance (ANOVA) with the Bonferroni post hoc test. Statistical differences between two groups were calculated using a two-tailed unpaired *t*-test. Differences were considered significant when $^{\#}p < 0.05$, $^{\#\#}p < 0.01$, $^{\#\#\#}p < 0.001$ or $^{*}p < 0.05$, $^{**}p < 0.01$, $^{***}p < 0.001$.

3. Results

3.1. Upregulation of FGF receptors (FGFRs) mRNA expression in cirrhosis patients

We first examined the mRNA expression levels of fibroblast growth factor receptors (FGFRs) and fibroblast growth factor 2 (FGF2) in human cirrhotic liver tissues using the publicly available human microarray datasets GSE6764 from the NCBI GEO database [26]. Patients were categorized into two groups: normal and cirrhosis representing normal and cirrhotic livers respectively. The available corresponding microarray datasets were analysed using an online database GEO2R. There are four known isoforms of FGFRs: FGFR1, FGFR2, FGFR3 and FGFR4, and all FGFRs are shown to be expressed in the liver [28]. Transcriptomic data analysis revealed a significant increase in the mRNA expression levels of FGFR1 ($p < 0.05$), FGFR2 ($p < 0.001$) and FGFR3 ($p < 0.05$) in the cirrhotic livers compared to the normal livers ($p < 0.05$) (Fig. 1A). However, no significant difference in FGFR4 mRNA expression ($p = 0.1037$) was observed in cirrhotic versus normal livers. Plasma levels of basic FGF (FGF2) were found to be significantly elevated with the progression of liver disease (chronic hepatitis > liver cirrhosis > hepatocellular carcinoma (HCC) [29]. However, no significant difference in FGF2 mRNA expression, in the analysed dataset

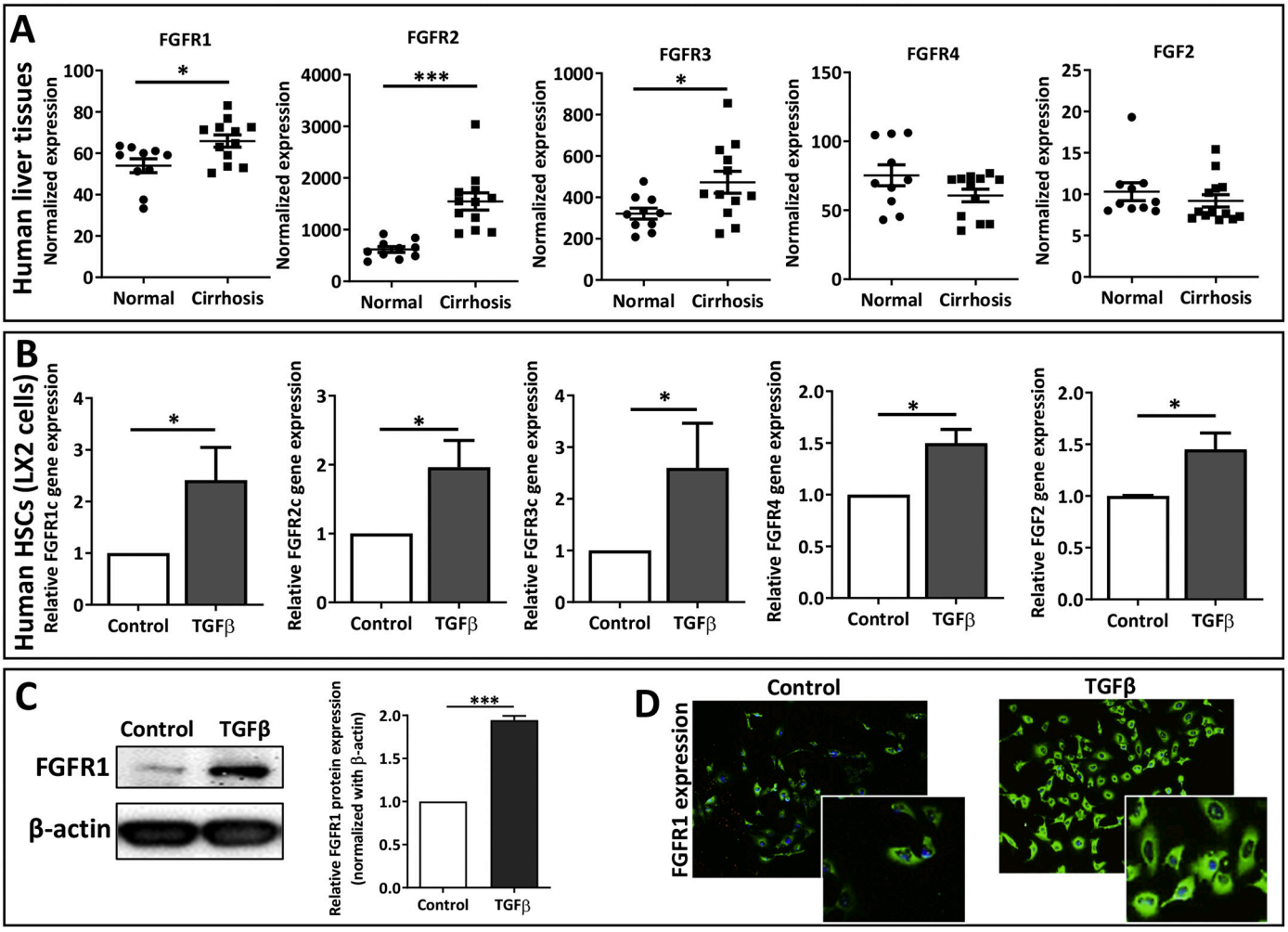

Fig. 1. Expression of fibroblast growth factor receptors (FGFR) and FGF2 in human cirrhotic livers and TGFβ-activated human hepatic stellate cells (HSCs, LX2 cells). (A) Normalized FGFR1, FGFR2, FGFR3, FGFR4 and FGF2 mRNA expression levels from publicly available human microarray datasets (GSE6764). Normal livers ($n = 10$) and cirrhosis livers ($n = 12$). (B) Relative mRNA expression (normalized with 18 s rRNA) of FGFR1c, FGFR2c, FGFR3c, FGFR4 and FGF2 in control and TGFβ-activated LX2 cells, $n = 6$. (C) Representative image and quantitative analysis of western blot showing expression of FGFR1 and β-actin, performed on control and TGFβ-activated LX2 cells, n = 6. (D) Representative immunofluorescent images showing expression of FGFR1 (green) in control and TGFβ-activated HSCs (LX2 cells). Blue staining represents DAPI-nuclear staining, $n = 3$. Graphs represent mean + SEM; statistical differences were calculated using two-tailed unpaired *t*-test, $^{*}P < 0.05$, $^{***}P < 0.001$. (For interpretation of the references to colour in this figure legend, the reader is referred to the web version of this article.)

GSE6764, was observed in the cirrhotic human livers as compared to the normal healthy livers (Fig. 1A).

3.2. Upregulation of FGFRs expression in vitro in human HSCs (LX2 cells)

FGFRs have shown to be expressed by hepatocytes and HSCs, and are involved in epithelium-mesenchymal paracrine signaling thereby regulating organogenesis [8]. During liver injury, different FGFs produced by HSCs bind and activate the FGFRs on hepatocytes, and hepatocyte-derived FGFs bind and activate FGFRs on HSCs thereby regulating hepatic fibrogenesis [9]. Here, we examined the expression levels of different FGF receptors and FGF2 in control and human HSCs activated by TGFβ since TGFβ is the major fibrogenic cytokine responsible for the activation and trans-differentiation of quiescent HSCs in the liver. We activated LX2 cells (a human HSC cell line) with 5 ng/mL of recombinant human TGFβ1 for 24 h and examined the mRNA expression levels of FGFRs and FGF2 in TGFβ-activated LX2 cells versus control LX2 cells. We observed that mRNA expression of the FGFRs isoforms: FGFR1c ($p < 0.05$), FGFR2c ($p < 0.05$), FGFR3c ($p < 0.05$) and FGFR4 ($p < 0.05$) was significantly upregulated in TGFβ-activated LX2 cells compared to control cells as shown in Fig. 1B. No significant differences in the mRNA expression for FGFR1b, FGFR2b, FGFR3b were observed in activated human HSCs [30]. Moreover, we found a significant increase in FGF2 mRNA levels (Fig. 1B), which is in accord with the recent study whereby induced FGF2 mRNA was observed in activated human HSCs [30]. Since FGF2 primarily interacts with FGFR1, overexpressed by human myofibroblasts [21], we assessed the protein expression of FGFR1 using western blot analysis and immunofluorescent staining in TGFβ-activated HSCs versus control cells. We found that FGFR1 was highly upregulated in the TGFβ-induced LX2 cells compared to control cells (Fig. 1C, D).

3.3. FGF2 inhibited collagen and α-SMA expression in TGFβ-activated human HSCs (LX2 cells) via pAKT signaling pathway

FGFs are categorized into seven subfamilies: FGF1, 4, 8, 9, 10, 11 and 19 as mentioned before [8,9]. Among other subfamilies, FGF1 subfamily, FGF1 and FGF2 have been investigated for their effects on HSCs and liver fibrogenesis [9]. In particular, FGF2 has been shown to regulate HSCs activation [9]. In this study, we investigated the effects of FGF2 on TGFβ-activated HSCs. Upon incubation with TGFβ, we observed a significant upregulation of major extracellular matrix (ECM)

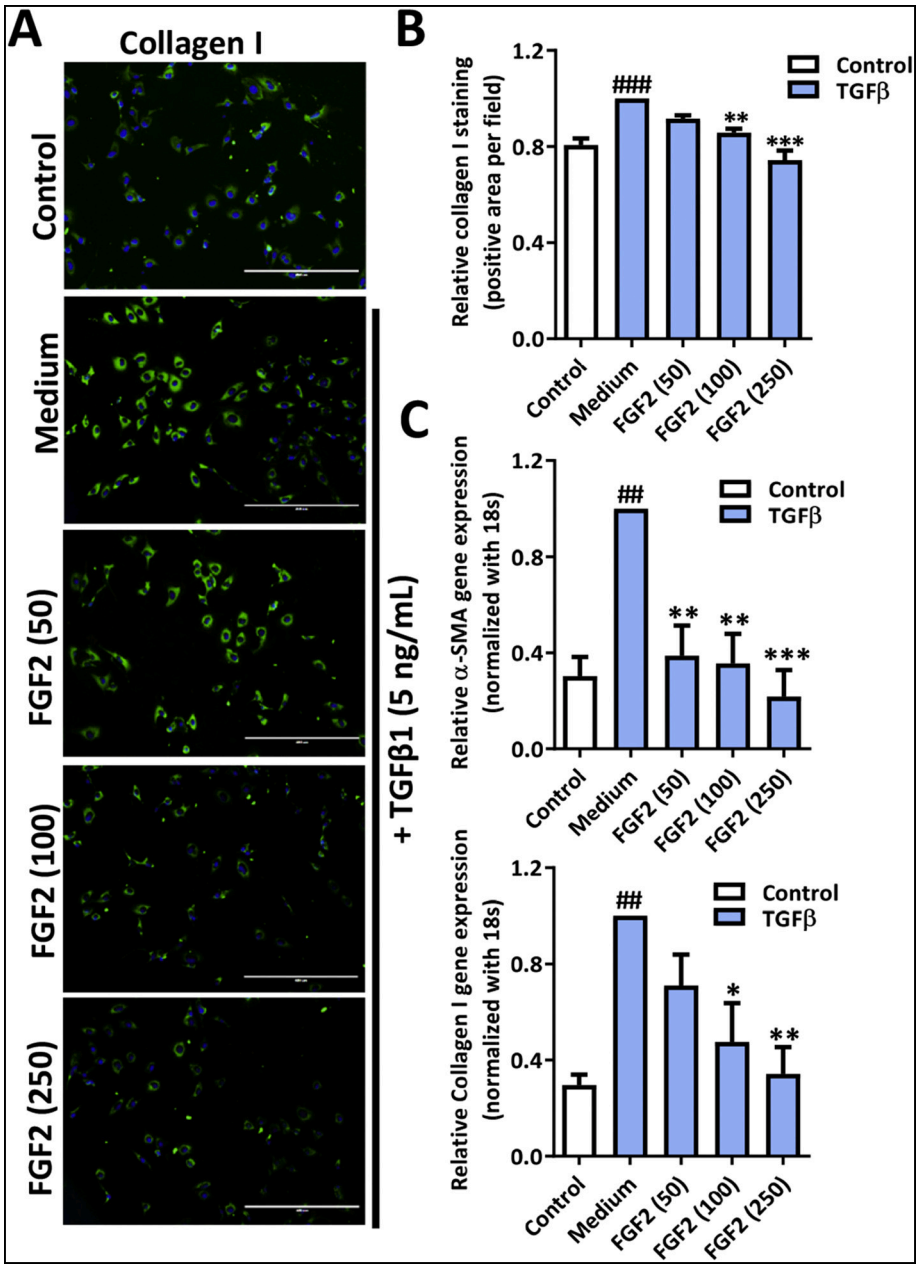

Fig. 2. Effects of FGF2 on collagen I and α-SMA expression on TGFβ-activated LX2 cells. (A) Representative immunofluorescent images and (B) quantitative analysis of collagen I (green colour) stained control and TGFβ-activated LX2 cells treated with medium alone or FGF2 (50, 100 and 250 ng/mL), $n = 7$. Blue staining represents DAPI-nuclear staining. (B) Relative gene expression analysis (normalized with 18 s rRNA) for α-SMA and collagen I as examined in control and TGFβ-activated LX2 cells treated with medium alone or FGF2 in different concentration (50, 100 and 250 ng/mL), $n = 4$. Graphs represent mean + SEM, statistical differences were calculated using one-way ANOVA with the Bonferroni post hoc test, $^{\#\#}P < 0.01$, $^{\#\#\#}P < 0.001$ represent significance versus control cells; $^{*}P < 0.05$, $^{**}P < 0.01$, $^{***}P < 0.001$ represent significance versus TGFβ-treated cells. (For interpretation of the references to colour in this figure legend, the reader is referred to the web version of this article.)

protein, collagen I and mRNA expression of major HSCs activation markers, alpha-smooth muscle actin (α-SMA), collagen I and TGFβ1, in TGFβ-activated LX2 compared to control LX2 cells. After treatment with increasing concentrations of FGF2, dose-dependent inhibition in collagen I protein expression and mRNA expression of α-SMA, collagen I and TGFβ1 was found (Fig. 2A-C and Fig. S1).

Moreover, FGF2-mediated dose-dependent inhibition of TGFβ-induced collagen I and α-SMA protein expression which was confirmed by western blot analysis (Fig. 3). We also investigated the possible mechanism of action underlying FGF2-mediated inhibitory effects on TGFβ-activated HSCs. Previously, it has been shown that FGF2 regulates proliferation, migration, and invasion of cancer cells through the phosphatidylinositol 3-kinase (PI3K)/AKT signaling pathway [31]. In an ischemia-reperfusion induced renal injury model, it has been demonstrated that selective inhibition of phosphatidylinositol 3-kinase (PI3K) [and mitogen-activated protein kinase kinase (MAPKK or MEK)] abolished the protective effects of FGF2 confirming an involvement of the PI3K/AKT (and MEK/ERK signaling pathways) in FGF2-mediated effects [17]. Moreover, activation of the PI3K/AKT signaling pathway, regulated by TGFβ, has been shown to stimulate collagen synthesis by fibroblasts in different fibrotic diseases e.g. by HSCs in hepatic fibrogenesis [32]. In this study, we examined the expression of p-AKT in control LX2 cells and TGFβ-activated LX2 cells treated without and with increasing concentrations of FGF2. We observed that TGFβ led to an increased expression of pAKT in LX2 cells which was dose-dependently inhibited with increasing concentrations of FGF2 (Fig. 3).

3.4. FGF2 inhibited TGFβ-induced migration and collagen gel contractility of human HSCs (LX2 cells)

Upon TGFβ activation, HSCs become highly migratory and contractile cells that drives the fibrotic alterations associated with chronic liver disease [3,6]. Therefore, we also assessed the effects of FGF2 on TGFβ-induced HSCs migration and contraction. We performed a scratch assay to assess HSCs migration and observed that TGFβ potentiated migration of HSCs which was significantly and dose-dependently inhibited by an increasing concentrations of FGF2 (Fig. 4A, C). We also examined the HSCs contraction using a 3D collagen gel contraction

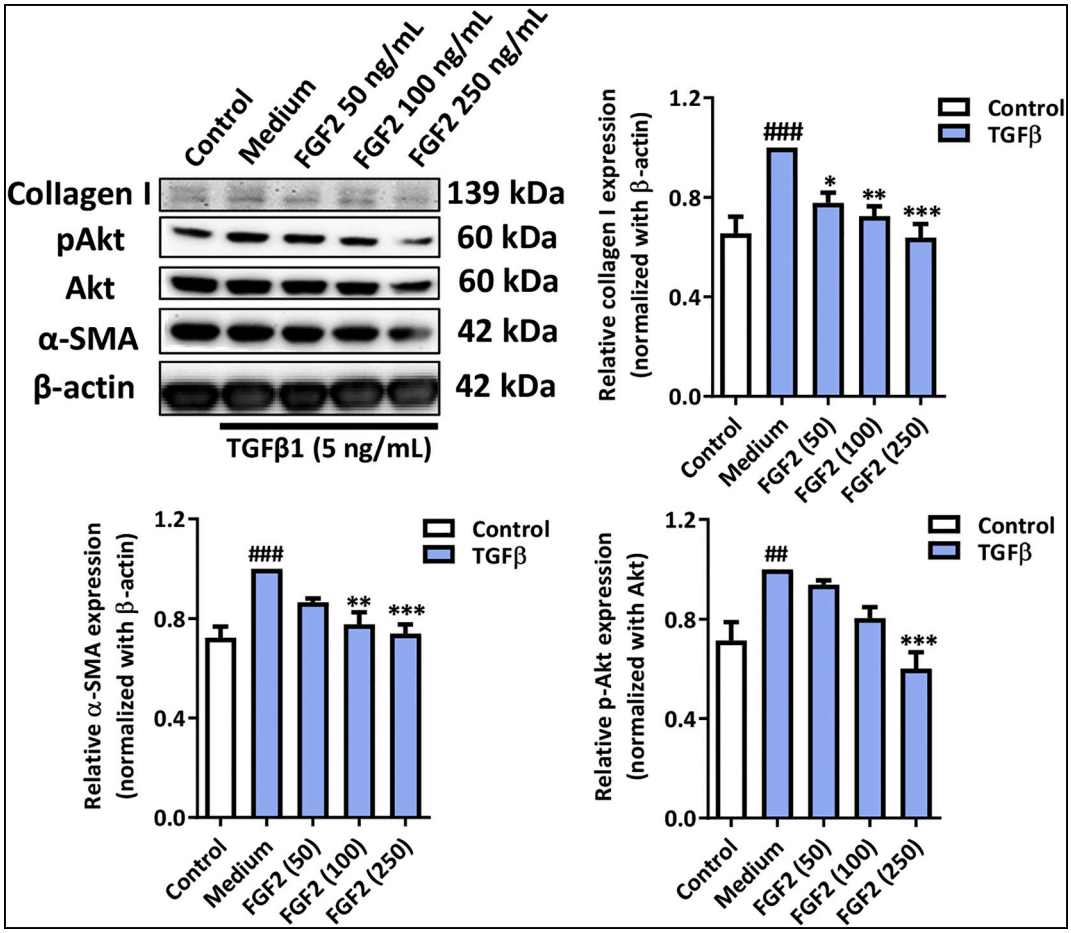

Fig. 3. FGF2 mediates the effects on TGFβ-activated LX2 cells via pAKT signaling pathway. Representative images and quantitative analysis of western blot depicting bands for collagen I, pAkt, Akt, α-SMA and β-actin, examined in control and TGFβ-activated LX2 cells treated with medium alone or increasing concentrations of FGF2 (50, 100 and 250 ng/mL), $n = 3$. Graphs represent mean + SEM, statistical differences were calculated using one-way ANOVA with the Bonferroni post hoc test, $^{\#\#}P < 0.01$, $^{\#\#\#}P < 0.001$ represent significance versus control cells; $^{*}P < 0.05$, $^{**}P < 0.01$, $^{***}P < 0.001$ represent significance versus TGFβ-treated cells.

assay and found that FGF2 dose-dependently decreased TGFβ-induced HSCs contraction (Fig. 4B, D). Finally, we analysed the effect of FGF2 on cell viability and observed no significant differences on cell viability with tested FGF2 concentrations (Fig. 4E).

3.5. Characterization of FGF2-SPIONs

After confirming the pharmacological effects of FGF2 in vitro on TGFβ-activated HSCs, we conjugated FGF2 protein to SPIONs. Biologics such as peptides and proteins have very short half-life and are highly prone to enzymatic degradation and therefore are rapidly eliminated from the body or degraded reducing their therapeutic efficacy [33]. Several strategies including nanocarriers-mediated peptide/protein drugs delivery have been evolved over years to protect them from degradation and to prolong their systemic half-life [34]. In this study, we used SPIONs to improve the half-life of FGF2 and target FGF2 to the livers. We conjugated FGF2 to dextran-coated PEG-COOH functionalized SPIONs using carbodiimide reaction chemistry as illustrated in a schematic picture in Fig. 5A.

We conjugated the cysteine part of the FGF2 to the functionalized SPIONs and left the FGF2 receptor-binding domain abide to interact with FGFR1 on the HSCs surface. The conjugation of FGF2 to SPIONs was confirmed by changes in size and zeta potential, and by dot-blot analysis. DLS measurements showed a slight increase in the mean hydrodynamic size of SPIONs after conjugation with FGF2 (95 nm FGF2-SPIONs versus 80 nm SPIONs) (Fig. 5B). We also observed an increase in the negative zeta potential) of the nanoparticles after FGF2 conjugation (mean value of about −10 mV for FGF2-SPIONs versus about −4 mV for SPIONs) (Fig. 5B). The successful conjugation of FGF2 to SPIONs was confirmed by a dot blot analysis using anti-FGF2 antibody (Fig. 5C). Based on the quantitative analysis of FGF2 and FGF2-SPIONs, about 82% of FGF2 was estimated to be conjugated to the SPIONs as derived from FGF2 standard curves presented in Fig. S2. Prussian Blue iron-staining and the respective quantitative analysis confirmed that about 88% SPIONs were recovered after conjugation due to the nanoparticle loss during the purification steps as determined by SPIONs standard curves presented in Fig. S2.

Quantitative analysis of dot blot FGF2 staining and iron staining (Fig. S2) suggested 93% conjugation of FGF2 to SPIONs indicating 4–5 FGF2 molecules per SPION. Finally, we characterized the binding and uptake of FGF2-SPIONs in TGFβ-activated LX2 cells. The result demonstrated an increase in binding and uptake of FGF2-SPIONs as compared to the unconjugated SPIONs (Fig. 5D).

Subsequently, we analysed the effect of FGF2-SPIONs and SPIONs on cell viability and observed no significant effects on cell viability with tested concentrations (up to 250 ng/mL) (Fig. 5E). FGF2-SPIONs were examined for long-term stability at 4 °C using DLS measurements (size) and dot blot (FGF2 conjugation/release) analysis. The results showed that FGF2-SPIONs retained their size and FGF2 conjugation after 4 weeks of storage at 4 °C.

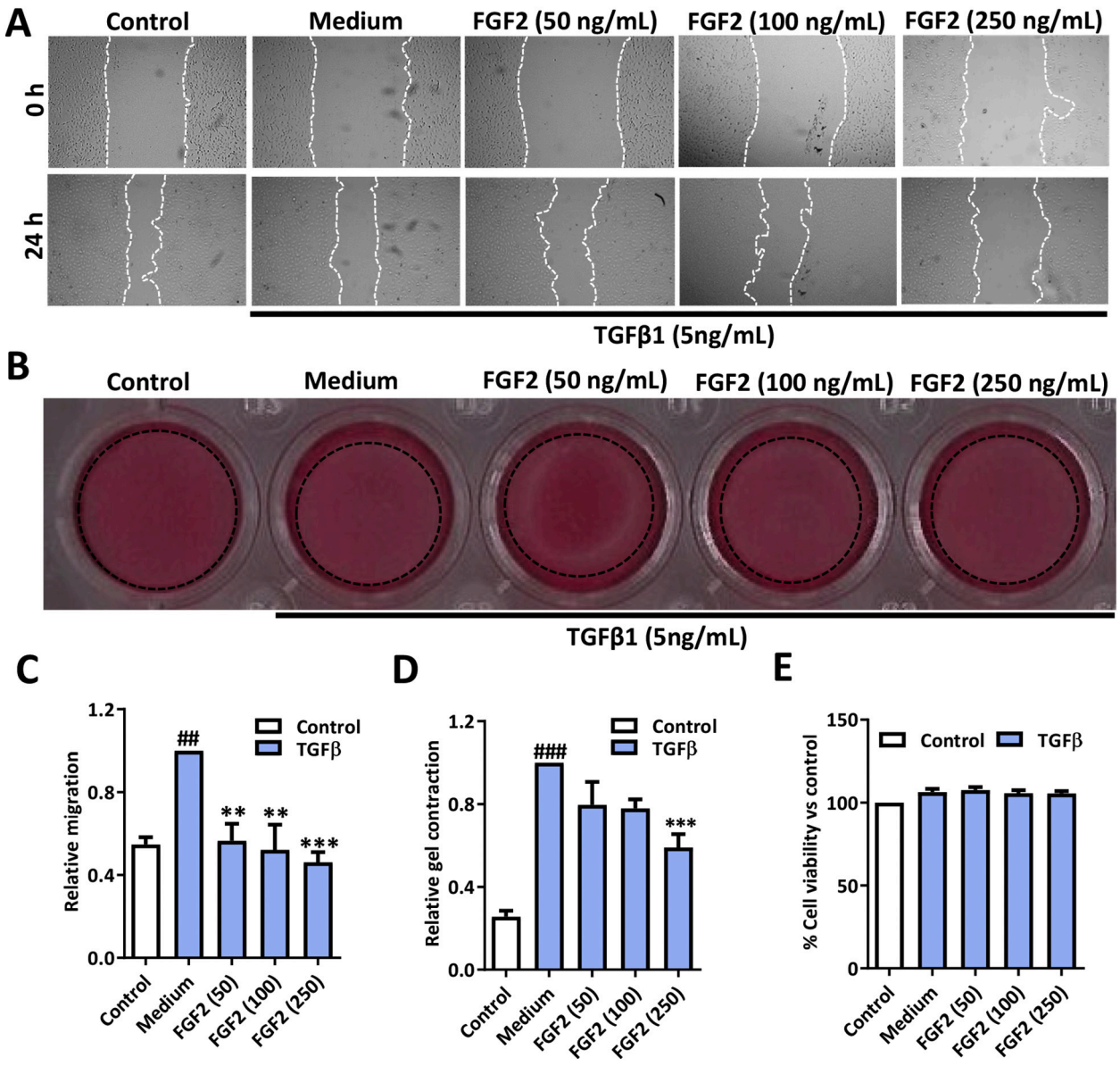

Fig. 4. Efficacy of FGF2 on TGFβ-induced migration and contractility of TGFβ-activated LX2 cells. (A) Representative images (at 0 and 24 h) and (C) quantitative analysis (after 24 h) of migration by control and TGFβ-induced LX2 cells treated with medium alone or FGF2 (50, 100 and 250 ng/mL). (B) Representative images (after 72 h) and (D) quantitative analysis of 3D collagen gel contraction by control and TGFβ-activated LX2 cells treated with medium alone or FGF2 (50, 100 and 250 ng/mL). (E) % cell viability of control cells and TGFβ-activated LX2 cells treated with medium alone or FGF2 (50, 100 and 250 ng/mL). Graphs represent mean + SEM, statistical differences were calculated using one-way ANOVA with the Bonferroni post hoc test, $^{\#\#}P < 0.01$, $^{\#\#\#}P < 0.001$ represent significance versus control cells; $^{**}P < 0.01$, $^{***}P < 0.001$ represent significance versus TGFβ-treated cells.

3.6. FGF2-SPIONs inhibited expression of fibrosis markers, migration, and contractility of human HSCs (LX2) in vitro

Following FGF2 conjugation to SPIONs, we examined whether FGF2 retains its pharmacological activity after chemical conjugation. To assess the effects of FGF2-SPIONs, we used 250 ng/mL FGF2 based on our previous dose-dependent studies (Figs. 2, 3, 4). We investigated the effects of FGF2-SPIONs on collagen I and α-SMA protein expression, and collagen I, α-SMA and TGFβ1 mRNA expression on TGFβ- activated LX2 cells and found that FGF2-SPIONs reduced both TGFβ-induced α-SMA and collagen I expression, and TGFβ1 mRNA expression (Fig. 6 and Fig. S3).

Collaborating with our previous results, FGF2-SPIONs also inhibited the protein expression of pAkt in TGFβ-activated LX2 cells (Fig. 6C, D). We further examined the effect of FGF2-SPIONs on TGFβ-induced HSCs migration and contraction and observed that FGF2-SPIONs attenuated TGFβ-induced HSCs migration (Fig. 7A) and contraction (Fig. 7B). The results clearly demonstrated that conjugation of FGF2 to SPIONs retained the pharmacological effects of FGF2 and showed similar or slightly improved HSCs inhibitory effects as compared to free unconjugated FGF2. Of note, SPIONs alone did not show significant inhibition of HSCs as also reported previously [25].

3.7. FGF2-SPIONs ameliorated fibrosis and inflammation in the CCl_4-induced acute liver injury mouse model

FGF2-SPIONs were subsequently evaluated for their therapeutic effects in the acute CCl_4-induced liver injury mouse model. Single CCl_4 administration resulted in an increased expression of intra-hepatic collagen I (major ECM marker indicative of HSCs activation and ECM production, and fibrogenesis) and increased F4/80 (macrophage marker indicative of macrophage-driven liver inflammation) expression

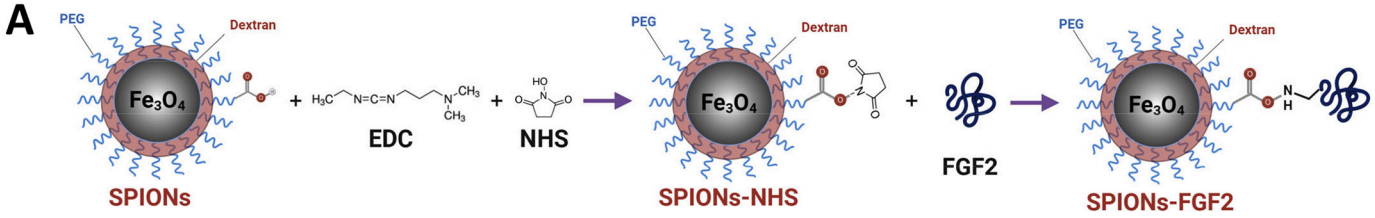

B

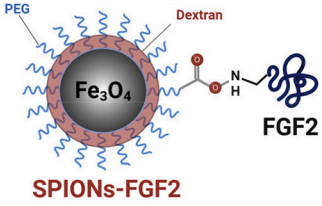

Nanoparticles	Size (nm)	PDI	Zeta potential (mV)
SPIONs	80.83 ± 1.23	0.157	- 3.83 ± 0.58
FGF2-SPIONS	94.60 ± 1.53	0.191	- 10.04 ± 0.73

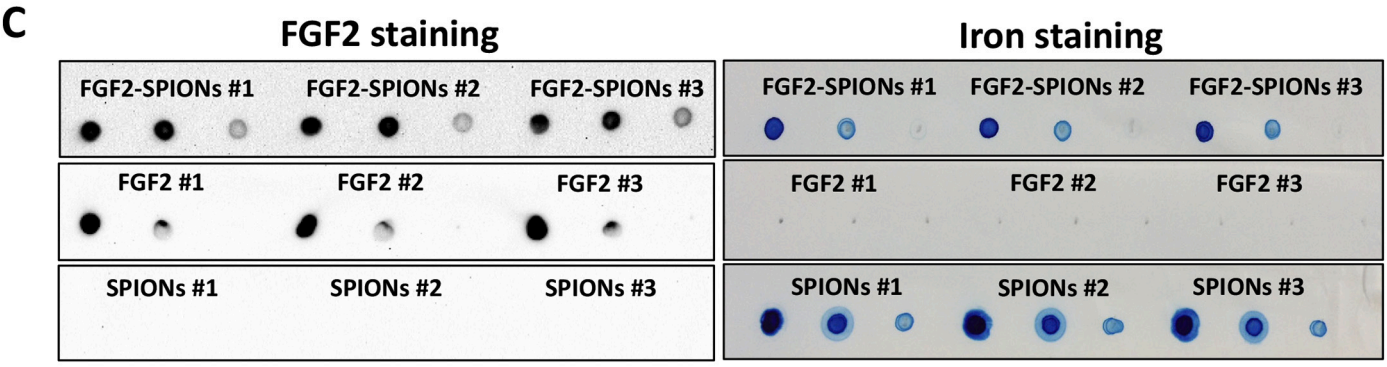

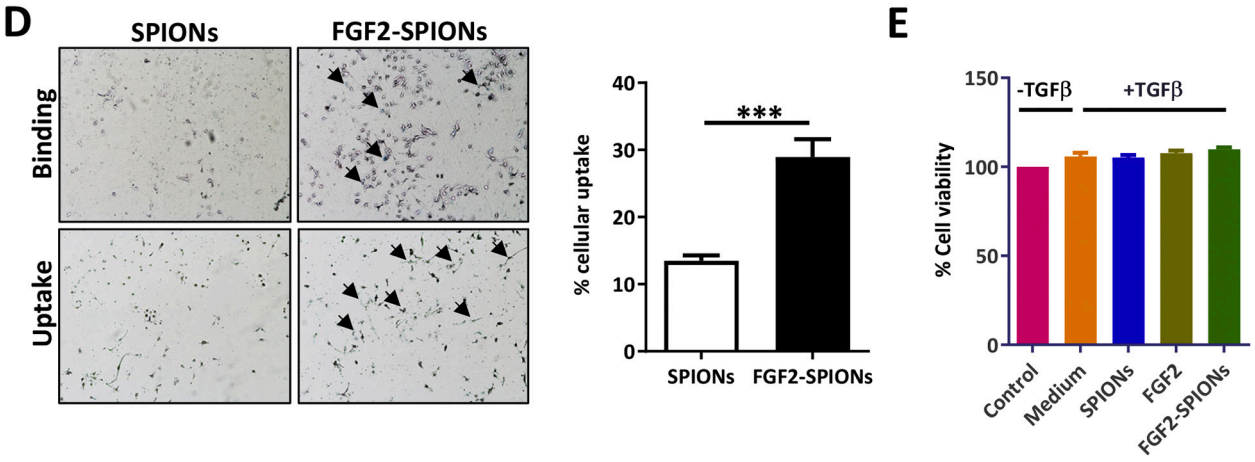

Fig. 5. Characterization and HSCs-specific binding/uptake of FGF2-SPIONs. (A) Schematic representation of FGF2 conjugation to SPION using carbodiimide chemistry. (B) Schematic of FGF2-SPIONs and table showing the hydrodynamic size, polydispersity index (PDI) and zeta potential of SPIONs and FGF2-SPIONs from $n = 3$ independent conjugations. (C) Dot blot image displaying FGF2 conjugation on SPIONs performed by FGF2 staining and SPIONs detection by Prussian Blue iron staining. FGF2-SPIONs, FGF2 and SPIONs were serially diluted and spotted on the membrane, thus the different dots in the figure represents the serial dilution of the respective samples. (D) Representative microscopic images and quantitative image analysis showing binding and uptake of FGF2-SPIONs versus SPIONs in TGFβ-activated LX2 cells, $n = 8$. (E) % cell viability of control LX2 cells and TGFβ-activated LX2 cells with and without SPIONs, FGF2, FGF2-SPIONs treatment, n = 8. Graphs represent mean + SEM; statistical differences were calculated using two-tailed unpaired *t*-test, $^{***}P < 0.001$. (For interpretation of the references to colour in this figure legend, the reader is referred to the web version of this article.)

in CCl_4-treated mice when compared with olive oil treated control mice. FGF2-SPIONs (and not free FGF2) significantly attenuated collagen I and F4/80 protein expression when compared with CCl_4 mice or CCl_4 mice treated with free FGF2 ($P < 0.05$) as shown in Fig. 8A, B. Furthermore, % liver weight (normalized with respective body weight) was found to be increased in CCl_4 mice and CCl_4 mice treated with free FGF2. Notably CCl_4 mice treated with FGF2-SPIONs showed significantly lowered % liver weights when compared with CCl_4 mice ($P < 0.001$), or CCl_4 mice treated with free FGF2 ($P < 0.01$) (Fig. 8C). We further examined the localization of FGF2-SPIONs in the fibrotic livers. Following Prussian blue iron staining of collagen-I stained liver sections, we observed localization of FGF2-SPIONs (stained with Prussian blue) in the fibrotic regions stained with collagen-I secreted by activated HSCs confirming HSCs-specific localization of FGF2-SPIONs in the fibrotic livers (Fig. S4). This observation aligns and supports our previous findings where we have shown an increased, possibly HSCs-specific, uptake of RLX-SPIONs (relaxin-conjugated SPIONs) in the fibrotic livers when compared to unconjugated

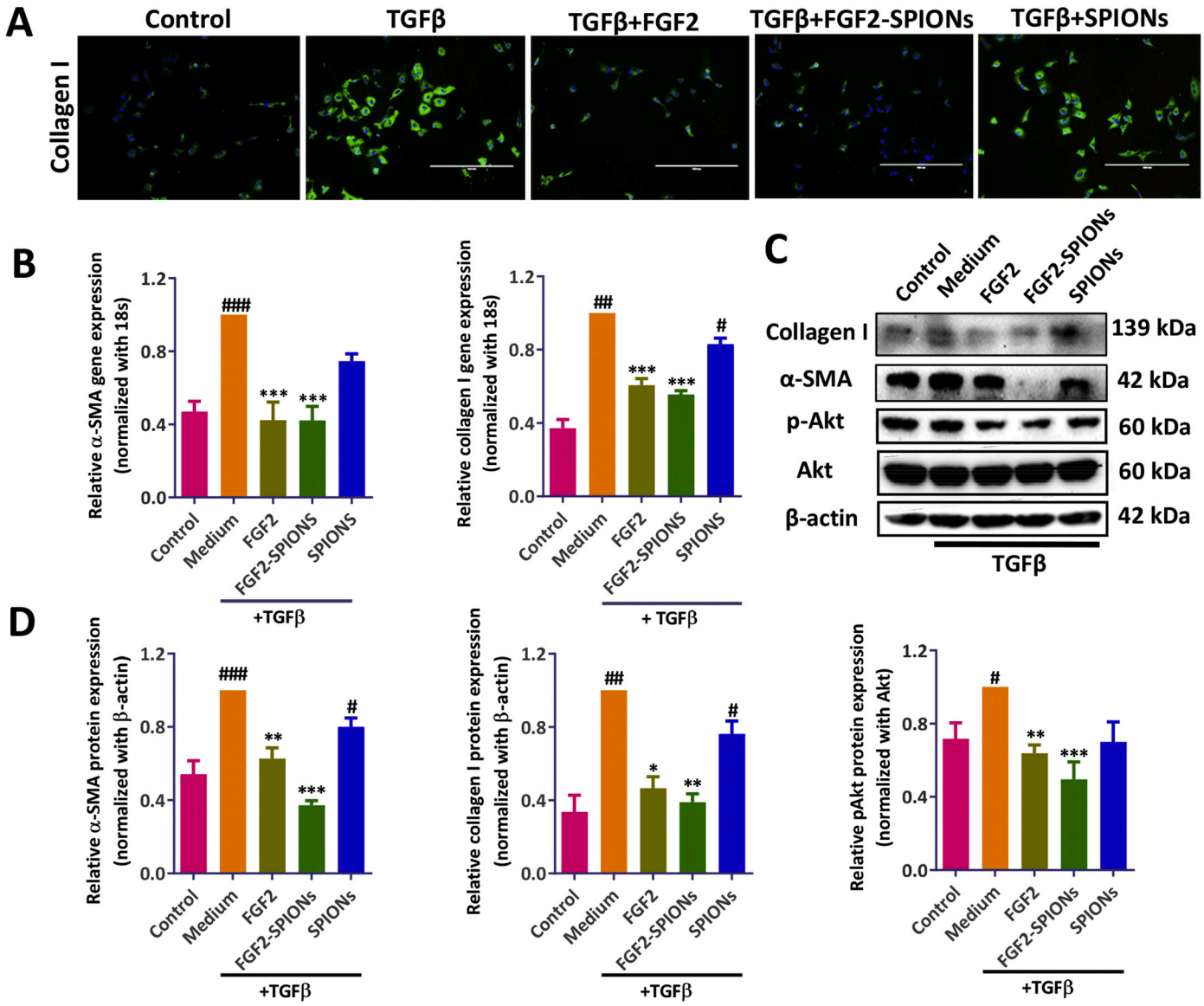

Fig. 6. Effects of FGF2-SPIONs on TGFβ-activated LX2 cells. (A) Representative immunofluorescent images ($n = 4$) and quantitative analysis of collagen I stained control and TGFβ-activated LX2 cells treated with medium alone, FGF2, FGF2-SPIONs or SPIONs. (B) Gene expression analysis for α-SMA and collagen I (normalized with 18 s rRNA) in control and TGFβ-activated LX2 cells treated with medium alone, FGF2, FGF2-SPIONs or SPIONs, $n = 6$. (C) Representative images and (D) quantitative analysis of western blot depicting bands for collagen I, pAkt, Akt, α-SMA and β-actin, examined in control and TGFβ-activated LX2 cells treated with medium alone, FGF2, FGF2-SPIONs or SPIONs, $n = 3$. Graphs represent mean + SEM, statistical differences were calculated using one-way ANOVA with the Bonferroni post hoc test, $^{\#}p < 0.05$, $^{\#\#}P < 0.01$, $^{\#\#\#}P < 0.001$ represent significance versus control cells; $^{*}P < 0.05$, $^{**}P < 0.01$, $^{***}P < 0.001$ represent significance versus TGFβ-treated cells.

SPIONs using MRI [25].

Finally, we examined plasma ALT levels and observed highly significant downregulation in ALT levels following treatment with FGF2-SPIONs when compared with CCl_4 mice ($P < 0.001$) or CCl_4 mice treated with free FGF2 ($P < 0.05$) (Fig. 8D). Based on the previous in vitro results and our previous studies [25,27,35] demonstrating that multiple administrations of SPIONs didn't show any beneficial therapeutic effects, SPIONs were not tested in vivo in the acute CCl_4-induced liver injury mouse model.

4. Discussion

In this study, we demonstrated an improved therapeutic efficacy of FGF2 after conjugation to SPIONs, as a promising approach for the treatment of liver fibrosis. We confirmed an upregulation of intrahepatic mRNA expression of FGFRs in cirrhotic patients and TGFβ-activated HSCs. We further observed an increased protein expression of FGFR1, a major FGF2-binding receptor in TGFβ-activated HSCs. Human recombinant FGF2 attenuated TGFβ-induced HSCs activation, collagen I production, migration and contraction mediated via the pAKT pathway. FGF2-conjugated SPIONs showed improved inhibition of TGFβ-activated HSCs in vitro, and ameliorated inflammation and collagen I production in vivo in the acute CCl_4-induced liver injury mouse model.

Acute liver injury is a transient wound healing response characterized by liver inflammation (increased infiltration and activation of macrophages) and fibrogenesis (enhanced activation of quiescent HSCs). When the injury persists, liver undergoes progressive scarring and degeneration in a process known as fibrosis. HSCs are the main pathogenic cells responsible for the production of abnormal fibrillar collagens in liver fibrosis. Therefore, substantial efforts have been made to target HSCs for the treatment of liver fibrosis which showed

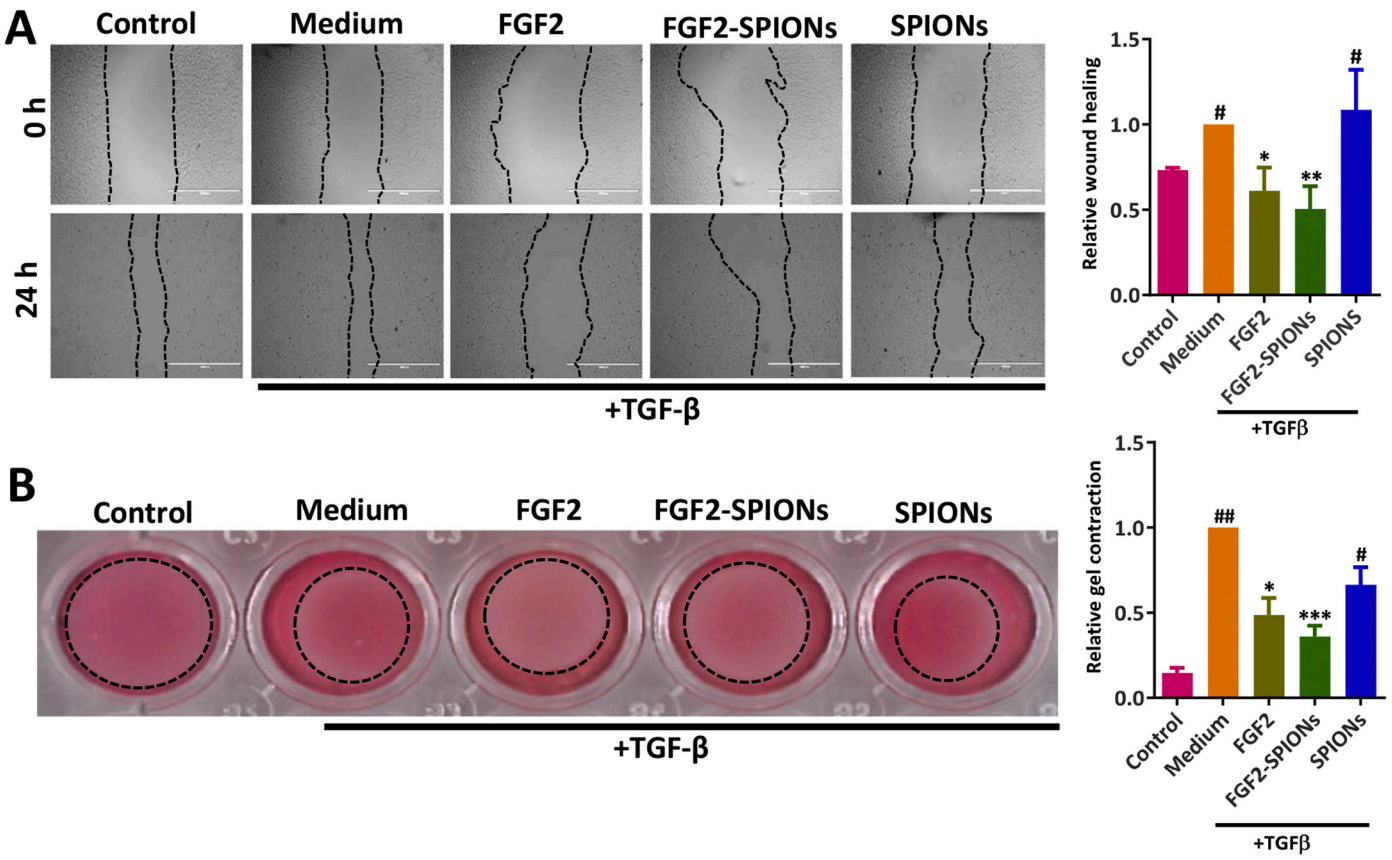

Fig. 7. Effects of FGF2-SPIONs on TGFβ-induced migration and contractility of human HSCs (LX2). (A) Representative images (at 0 and 24 h) and quantitative analysis (after 24 h) of migration by control and TGFβ-induced LX2 cells treated with medium alone, FGF2, FGF2-SPIONs or SPIONs. (B) Representative images (after 72 h) and quantitative analysis of 3D collagen gel contraction containing control and TGFβ-activated LX2 cells treated with medium alone, FGF2, FGF2-SPIONs or SPIONs, $n = 6$. Graphs represent mean + SEM, statistical differences were calculated using one-way ANOVA with the Bonferroni post hoc test. $\#P < 0.05$, ##P < 0.05 versus control LX2 cells; *P < 0.05, $^{**}P < 0.01$, $^{***}P < 0.001$ versus TGFβ-treated LX2 cells.

promising results [3–5,7]. Upon hepatocellular injury, HSCs are activated in the presence of growth factors, particularly TGFβ, that results in activation, proliferation, migration, contraction and collagen production by HSCs. Activation of HSCs is regulated by several growth factors and signaling pathways [3,4,6]. Among others, FGFs have also been shown to regulate HSCs [13], in particular FGF2 that has been shown to possess both pro- and anti-fibrotic effects [9,13]. In the present study, we found that exogenous low-molecular weight FGF2 attenuated HSCs activation, migration, contraction and collagen expression. Our results are in complete agreement with a study where high- and low-molecular weight FGF2 isoforms were compared and demonstrated that low-molecular weight FGF2, as also used in this study, potently ameliorated HSCs activation [15].

FGF2 can bind to different FGFR receptors with varying affinity. However, it mainly interacts with FGFR1 that has shown to be overexpressed on HSCs [21]. In this study, we also assessed the expression levels of different types of FGFRs in human cirrhosis and in TGFβ-activated human HSCs. Interestingly we found that almost all of the different FGFRs (except FGFR4) were upregulated in human cirrhotic livers. FGFR1c, FGFR2c, FGFR3c and FGFR4 mRNA levels were upregulated in TGFβ-activated human HSCs, and FGFR1 protein was highly expressed on TGFβ-activated human HSCs. Although several mechanisms have been proposed with regard to FGF2-FGFR1 [13,15,36], in this study we found an involvement of the PI3K/AKT signaling pathway since pAKT expression was significantly dose-dependently inhibited by an increasing concentrations of FGF2. These results corroborate with previous reports where selective inhibition of the PI3K/AKT signaling pathway was shown to abrogate the protective functions of FGF2 [13,17,31,32].

Our results confirmed the anti-fibrotic effects of FGF2. However FGF2, like other biologics, has several limitations such as short systemic half-life and susceptibility to enzymatic degradation thereby reduced stability [22]. rFGF2, when administered together with heparin, showed improved systemic circulation of FGF2 with slower clearance of heparin/rFGF-2 complexes [22]. Nanotechnological advancements in the last decades have improved the pharmacokinetics and targeted delivery of biologics e.g. using nanocarriers [33,37]. SPIONs provide several other advantages such as a small size and dextran-PEG surface coating for evading the mononuclear phagocytic system (MPS), and a large surface area allowing surface conjugation of biologics and detection using MRI [23,37,38].

FGF2 has been shown to possess anti-fibrotic effects as also reported by others [13,14,15,21,36]. In this study, by coupling FGF2 to the SPIONs, we aimed to enhance the systemic half-life and stability, and improve the targeting of FGF2 to the liver. Following successful synthesis of FGF2-SPIONs, we confirmed the biological activity of FGF2, and found that FGF2-SPIONs showed enhanced inhibition of HSCs activation, migration, contraction and collagen production, most likely, due to the increased FGF2 stability. Subsequently, we investigated the effects of FGF2 and FGF2-SPIONs in the acute CCl_4-induced liver injury mouse model. We found that two doses of 250 ng/dose/mouse FGF2-SPIONs attenuated fibrosis and inflammation in the early liver fibrogenesis model as confirmed by reduced collagen I (ECM) expression and F4/80 (macrophage) expression respectively. FGF2, in unconjugated free didn't show the significant inhibition in fibrogenesis in vivo at the tested doses. These results suggests that SPIONs improved the half-life and possibly liver accumulation and HSCs-specific targeting, and stability of FGF2 resulting in improved biological activity of

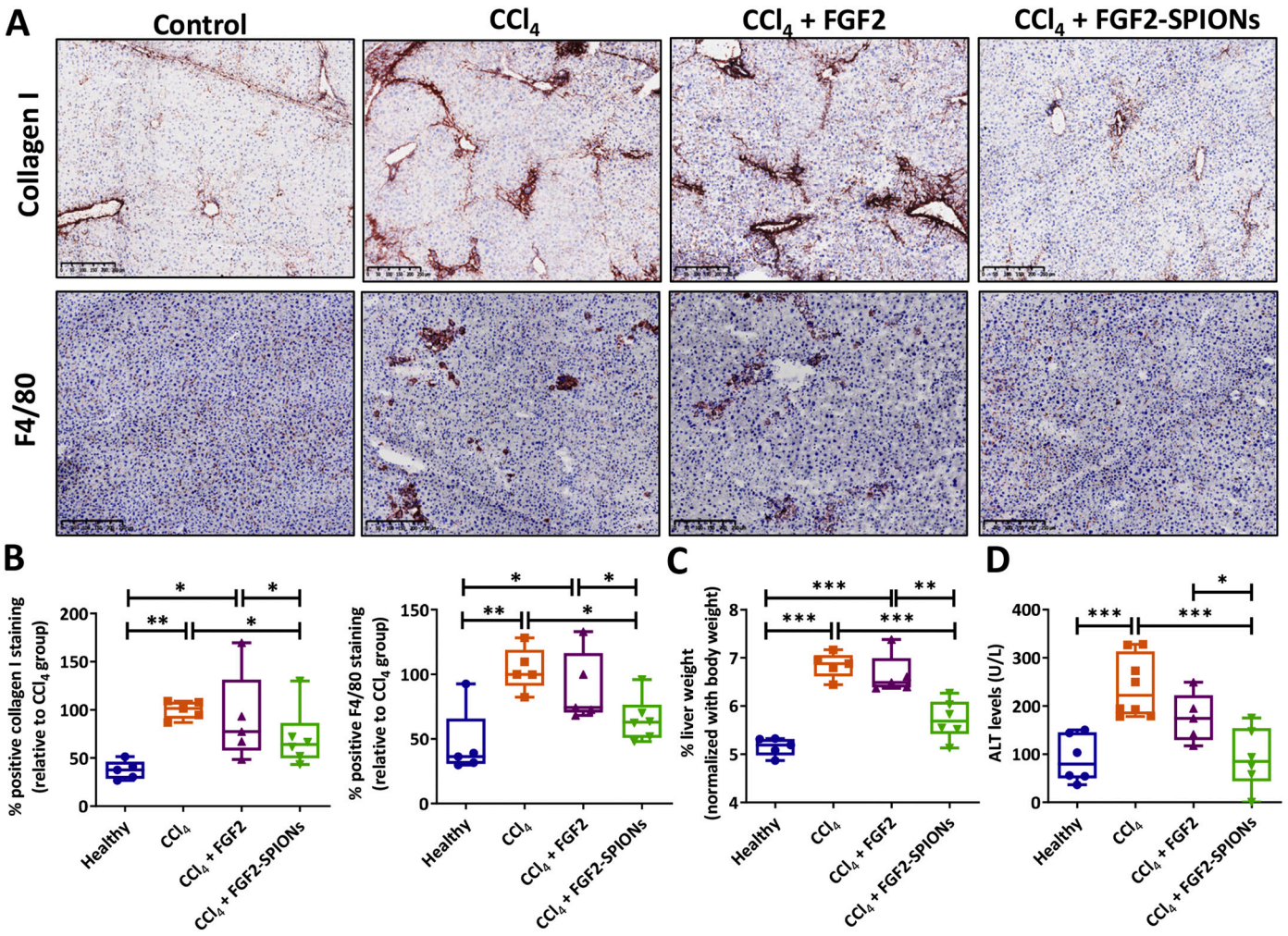

Fig. 8. Effects of FGF2-SPIONs in CCl_4-induced acute liver injury mouse model. (A) Representative images and (B) quantitative analysis of collagen I (ECM marker) and F4/80 (macrophage marker) stained liver sections from control group ($n = 6$), CCl_4 group (CCl_4 mice treated with PBS, $n = 5$), CCl_4 + FGF2 group (CCl_4 mice treated with free FGF2, n = 5), and CCl_4 + FGF2-SPIONs group (CCl_4 mice treated with FGF2-SPIONs, n = 6). (C) % liver weights (normalized with respective body weights) from control group (n = 6), CCl_4 group (CCl_4 mice treated with PBS, n = 5), CCl_4 + FGF2 group (CCl_4 mice treated with free FGF2, n = 5), and CCl_4 + FGF2-SPIONs group (CCl_4 mice treated with FGF2-SPIONs, n = 6). (D) Alanine aminotransferases (ALT) levels (U/l) as analysed in the plasma from different treatment groups. (B-D): Each symbol represents individual mice. Graphs represent mean ± SEM, statistical differences were calculated using one-way ANOVA with the Bonferroni post hoc test. *P < 0.05, **P < 0.01, ***P < 0.001.

FGF2 in vivo. Since FGF2 is also known to be involved in liver homeostasis, tissue repair and regeneration [11,40,41], it is also possible that FGF2-SPIONs positively improve hepatocyte proliferation and hence promote liver regeneration. To our best knowledge, this is the first study that explore the delivery of FGF2 to the diseased liver. However, this study has been performed in acute liver injury (early liver fibrosis) model that does not correspond to the clinical situation. Patients normally presents to the clinic when liver damage progresses to cirrhosis associated with liver dysfunction. Nevertheless, this study provides the first proof-of-concept results highlighting that FGF2-SPIONs can be a promising therapeutic approach, and therefore should to be further explored in an advanced models of liver cirrhosis.

In conclusion, this study demonstrates that SPIONs-mediated delivery of FGF2 potentiates the therapeutic efficacy of FGF2 in vitro and in vivo thereby suggesting FGF2-SPIONs as a potential therapeutic approach for the treatment of liver fibrosis. Moreover, SPIONs also provides a possibility for MRI-based diagnosis therefore may also provide a personalized theranostic approach with combined therapy and diagnosis for personalized disease management. Altogether, this study presents a novel approach for the delivery of FGF2 as an effective treatment of liver fibrosis.

Financial support

This study was supported by the Indonesian Endowment Fund for Education from the Republic of Indonesia (Lembaga Pengelola Dana Pendidikan/LPDP) and the University of Twente, The Netherlands.

Declaration of Competing Interest

The authors have no other relevant affiliations or financial involvement with any organization or entity with a financial interest in or financial conflict with the subject matter or materials discussed in the manuscript apart from those disclosed.

Appendix A. Supplementary data

Supplementary data to this article can be found online at https://doi.org/10.1016/j.jconrel.2020.09.041.

References

[1] S.K. Asrani, H. Devarbhavi, J. Eaton, P.S. Kamath, Burden of liver diseases in the

world, J. Hepatol. 70 (2019) 151–171.
[2] R. Bataller, D.A. Brenner, Liver fibrosis, J. Clin. Investig. 115 (2005) 209–218.
[3] S.L. Friedman, Mechanisms of hepatic fibrogenesis, Gastroenterology 134 (2008) 1655–1669.
[4] R. Bansal, B. Nagorniewicz, J. Prakash, Clinical advancements in the targeted therapies against liver fibrosis, Mediat. Inflamm. 2016 (2016) 7629724.
[5] D. Schuppan, Y.O. Kim, Evolving therapies for liver fibrosis, J. Clin. Invest. 123 (2013) 1887–1901.
[6] S.L. Friedman, Hepatic stellate cells: protean, multifunctional, and enigmatic cells of the liver, Physiol. Rev. 88 (2008) 125–172.
[7] S. Yazdani, R. Bansal, J. Prakash, Drug targeting to myofibroblasts: implications for fibrosis and cancer, Adv. Drug Deliv. Rev. 121 (2017) 101–116.
[8] D.M. Ornitz, N. Itoh, The fibroblast growth factor signaling pathway, Wiley Interdiscip. Rev. Dev. Biol. 4 (2015) 215–266.
[9] J.D. Schumacher, G.L. Guo, Regulation of hepatic stellate cells and Fibrogenesis by fibroblast growth factors, Biomed. Res. Int. 2016 (2016) 8323747.
[10] C.M. Teven, E.M. Farina, J. Rivas, R.R. Reid, Fibroblast growth factor (FGF) signaling in development and skeletal diseases, Genes Dis. 1 (2014) 199–213.
[11] S.M. Tsai, D.W. Liu, W.P. Wang, Fibroblast growth factor (Fgf) signaling pathway regulates liver homeostasis in zebrafish, Transgenic Res. 22 (2013) 301–314.
[12] A. Bikfalvi, S. Klein, G. Pintucci, D.B. Rifkin, Biological roles of fibroblast growth factor-2, Endocr. Rev. 18 (1997) 26–45.
[13] D.M. Dolivo, S.A. Larson, T. Dominko, Fibroblast growth factor 2 as an Antifibrotic: antagonism of Myofibroblast differentiation and suppression of pro-fibrotic gene expression, Cytokine Growth Factor Rev. 38 (2017) 49–58.
[14] C. Yu, F. Wang, C. Jin, X. Huang, D.L. Miller, C. Basilico, W.L. McKeehan, Role of fibroblast growth factor type 1 and 2 in carbon tetrachloride-induced hepatic injury and fibrogenesis, Am. J. Pathol. 163 (2003) 1653–1662.
[15] R.L. Pan, L.X. Xiang, P. Wang, X.Y. Liu, L. Nie, W. Huang, J.Z. Shao, Low-molecular-weight fibroblast growth factor 2 attenuates hepatic fibrosis by epigenetic down-regulation of Delta-like1, Hepatology 61 (2015) 1708–1720.
[16] H.Y. Koo, L.M. El-Baz, S. House, S.N. Cilvik, S.J. Dorry, N.M. Shoukry, M.L. Salem, H.S. Hafez, N.O. Dulin, D.M. Ornitz, R.D. Guzy, Fibroblast growth factor 2 decreases bleomycin-induced pulmonary fibrosis and inhibits fibroblast collagen production and myofibroblast differentiation, J. Pathol. 246 (2018) 54–66.
[17] X. Tan, Q. Tao, G. Li, L. Xiang, X. Zheng, T. Zhang, C. Wu, D. Li, Fibroblast growth factor 2 attenuates renal ischemia-reperfusion injury via inhibition of endoplasmic reticulum stress, Front Cell Dev. Biol. 8 (2020) 147.
[18] A.N. Plotnikov, J. Schlessinger, S.R. Hubbard, M. Mohammadi, Structural basis for FGF receptor dimerization and activation, Cell 98 (1999) 641–650.
[19] A. Chellaiah, W. Yuan, M. Chellaiah, D.M. Ornitz, Mapping ligand binding domains in chimeric fibroblast growth factor receptor molecules. Multiple regions determine ligand binding specificity, J. Biol. Chem. 274 (1999) 34785–34794.
[20] A.N. Plotnikov, S.R. Hubbard, J. Schlessinger, M. Mohammadi, Crystal structures of two FGF-FGFR complexes reveal the determinants of ligand-receptor specificity, Cell 101 (2000) 413–424.
[21] J. Rosenbaum, S. Blazejewski, A.-M. Preaux, A. Mallat, D. Dhumeaux, P. Mavier, Fibroblast growth factor 2 and transforming growth factor b1 interactions in human liver myofibroblast, Gastroenterology 109 (1995) 1986–1996.
[22] M.A. Bush, E. Samara, M.J. Whitehouse, C. Yoshizawa, D.L. Novicki, M. Pike, R.J. Laham, M. Simons, N.A. Chronos, Pharmacokinetics and pharmacodynamics of recombinant FGF-2 in a phase I trial in coronary artery disease, J. Clin. Pharmacol. 41 (2001) 378–385.
[23] J.E. Rosen, L. Chan, D.B. Shieh, F.X. Gu, Iron oxide nanoparticles for targeted cancer imaging and diagnostics, Nanomedicine 8 (2012) 275–290.
[24] C. Tassa, S.Y. Shaw, R. Weissleder, Dextran-coated iron oxide nanoparticles: a versatile platform for targeted molecular imaging, molecular diagnostics, and therapy, Acc. Chem. Res. 44 (2011) 842–852.
[25] B. Nagorniewicz, D.F. Mardhian, R. Booijink, G. Storm, J. Prakash, R. Bansal, Engineered Relaxin as theranostic nanomedicine to diagnose and ameliorate liver cirrhosis, Nanomedicine 17 (2019) 106–118.
[26] E. Wurmbach, Y.B. Chen, G. Khitrov, W. Zhang, S. Roayaie, M. Schwartz, I. Fiel, S. Thung, V. Mazzaferro, J. Bruix, E. Bottinger, S. Friedman, S. Waxman, J.M. Llovet, Genome-wide molecular profiles of HCV-induced dysplasia and hepatocellular carcinoma, Hepatology 45 (2007) 938–947.
[27] D.F. Mardhian, A. Vrynas, G. Storm, R. Bansal, J. Prakash, FGF2 engineered SPIONs attenuate tumor stroma and potentiate the effect of chemotherapy in 3D heterospheroidal model of pancreatic tumor, Nanotheranostics 4 (2020) 26–39.
[28] S.E. Hughes, Differential expression of the fibroblast growth factor receptor (FGFR) multigene family in normal human adult tissues, J. Histochem. Cytochem. 45 (1997) 1005–1019.
[29] K. Jim-No, M. Tanimizu, I. Hyodo, F. Kurimoto, T. Yamashita, Plasma level of basic fibroblast growth factor increases with progression of chronic liver disease, J. Gastroenterol. 32 (1997) 119–121.
[30] T. Seitz, K. Freese, P. Dietrich, W.E. Thasler, A. Bosserhoff, C. Hellerbrand, Fibroblast growth factor 9 is expressed by activated hepatic stellate cells and promotes progression of hepatocellular carcinoma, Sci. Rep. 10 (2020) 4546.
[31] H. Shi, J. Xu, R. Zhao, H. Wu, L. Gu, Y. Chen, FGF2 regulates proliferation, migration, and invasion of ECA109 cells through PI3K/Akt signalling pathway in vitro, Cell Biol. Int. 40 (2016) 524–533.
[32] M.K. Son, Y.L. Ryu, K.H. Jung, H. Lee, H.S. Lee, H.H. Yan, H.J. Park, J.K. Ryu, J.K. Suh, S. Hong, S.S. Hong, HS-173, a novel PI3K inhibitor, attenuates the activation of hepatic stellate cells in liver fibrosis, Sci. Rep. 3 (2013) 3470.
[33] B.J. Bruno, G.D. Miller, C.S. Lim, Basics and recent advances in peptide and protein drug delivery, Ther. Deliv. 4 (2013) 1443–1467.
[34] D.S. Pisal, M.P. Kosloski, S.V. Balu-Iyer, Delivery of therapeutic proteins, J. Pharm. Sci. 99 (2010) 2557–2575.
[35] D.F. Mardhian, G. Storm, R. Bansal, J. Prakash, Nano-targeted relaxin impairs fibrosis and tumor growth in pancreatic cancer and improves the efficacy of gemcitabine in vivo, J. Control. Release 290 (2018) 1–10.
[36] M. Sato-Matsubara, T. Matsubara, A. Daikoku, Y. Okina, L. Longato, K. Rombouts, L.T.T. Thuy, J. Adachi, T. Tomonaga, K. Ikeda, K. Yoshizato, M. Pinzani, N. Kawada, Fibroblast growth factor 2 (FGF2) regulates cytoglobin expression and activation of human hepatic stellate cells via JNK signaling, J. Biol. Chem. 292 (2017) 18961–18972.
[37] M. Arruebo, R. Fernández-Pacheco, M.R. Ibarra, J. Santamaría, Magnetic nanoparticles for drug delivery, Nano Today 2 (2007) 22–32.
[38] R. Tietze, J. Zaloga, H. Unterweger, S. Lyer, R.P. Friedrich, C. Janko, M. Pottler, S. Durr, C. Alexiou, Magnetic nanoparticle-based drug delivery for cancer therapy, Biochem. Biophys. Res. Commun. 468 (2015) 463–470.
[40] L. Maddaluno, C. Urwyler, S. Werner, Fibroblast growth factors: key players in regeneration and tissue repair, Development 144 (2017) 4047–4060.
[41] Y.R. Yun, J.E. Won, E. Jeon, S. Lee, W. Kang, H. Jo, J.H. Jang, U.S. Shin, H.W. Kim, Fibroblast growth factors: biology, function, and application for tissue regeneration, J. Tissue Eng. 2010 (2010) 218142.